SSRG International Journal of Electrical and Electronics Engineering
ISSN: 2348-8379/ https://doi.org/10.14445/23488379/IJEEE-V11I10P116

Volume 11 Issue 10, 156-167, October 2024

Original Article

Cat Swarm Optimized PI Controller Design for Wind Energy-Based Switched Reluctance Generator

N. Rathika[1*], S. Gomathi[2], A.A. Mohamed Faizal[3], R. Hemalatha[4], S. Marisargunam[5], A. Wisemin Lins[6]

[1]*Department of Electrical and Electronics Engineering, Mahendra Institute of Technology, Tamilnadu, India.*
[2]*Department of Electrical and Electronics Engineering, St. Joseph's College of Engineering, Tamilnadu, India.*
[3]*Department of Electrical and Electronics Engineering, V V College of Engineering, Tamilnadu, India.*
[4]*Department of Electrical and Electronics Engineering, Saveetha Engineering College, Tamilnadu, India.*
[5]*Department of Electrical and Electronics Engineering, PSN College of Engineering and Technology, Tamilnadu, India.*
[6]*Department of Electrical and Electronics Engineering, Vels Institute of Science Technology and Advanced Studies, Tamilnadu, India.*

**Corresponding Author : rathika.nsd@gmail.com*

Received: 11 August 2024 Revised: 10 September 2024 Accepted: 11 October 2024 Published: 30 October 2024

Abstract *- The ever-growing environmental concerns have led to a renewed interest in Renewable Energy Sources (RES), which provide clean, abundant power for long-term sustainable development. Wind power gained particular attention because of its relative availability and low cost, mainly for grid applications. In these circumstances, for wind energy conversion systems, Switched Reluctance Generators (SRGs) are developed in this work, which make sense because of their resilience, wide speed range, ease of maintenance, and ability to function in challenging conditions. To manage the speed of SRG by integrating a Proportional Integral (PI) controller, which adjusts the output current of Bridge Resonant (BR) converters (n+1 diode and n+1 semiconductor system. The PWM rectifier is adopted for converting the AC-DC supply, and a PWM generator (Hysteresis controller) is implemented to regulate a Voltage Source Inverter (VSI) by creating switching pulses for the device by instantaneously comparing the grid current and the reference current. Furthermore, the Cat Swarm Optimization technique is developed for tuning the PI controller, which boosts the performance and efficiency of the controller. Consequently, the grid synchronization is attained by the combined function of the PWM generator and three-phase Voltage Source Converter VSI with the PI controller. The proposed approach is executed in MATLAB, and a comparison with the traditional methods is carried out to show the method's proficiency. At last, the controller achieves tremendous performance for grid application in terms of low THD and settling time.*

Keywords *- BR converter, Cat Swarm Optimized PI controller, Hysteresis controller, RES, SRG, PI controller, Wind energy system.*

1. Introduction

Over the past few decades, the finite supply of fossil fuels and the greenhouse gas emissions they produce through burning have drawn the attention of many countries worldwide [1]. Consequently, there has been a notable surge in interest in RES, which has been the subject of many governmental initiatives and subsidies. Under these conditions, wind energy initially appeared as a practical means of converting RES in the 1980s [2]. Over the last 20 years, it has undergone a substantial transformation as a result of advancements in power electronics. Small-scale wind power systems are becoming more and more common in distant locations compared to large-scale wind power generating systems because of their advantages in compact size, simple construction, and simple control [3, 4]. Various generator types are utilized in small-scale wind power systems, including Permanent Magnet Synchronous Generators (PMSG), Silicon Rectifier Self-Excited Synchronous Generators (SRSEG) and DC generators. Initially, DC motors were mostly utilized for ease of power storage, but they required a lot of upkeep. PMSGs are renowned for their excellent efficiency [5, 6]. However, there are several difficulties when it comes to poorly functioning small-scale wind power-producing systems [7]. The permanent magnet, which provides the primary magnetic field for PMSG, is fixed, and its terminal voltage varies based on changes in load conditions. As a result, in the event of an unexpected change in wind speed, PMSG's ability to regulate voltage under difficult operating conditions is low, it is hard to achieve speed increases and feeble magnetism, and the voltage of the motor will increase unexpectedly or possibly break through the insulation and burn down [8, 9]. A small-scale wind system

that uses PMSG is not consistent enough to satisfy practical needs, and its poor fault tolerance suggests that the system's cost will rise as a result of the high cost of operation and maintenance in remote regions [10]. Self-excited synchronous generators with silicon rectifiers require a lot of maintenance due to their intricate design [11]. Consequently, the SRG generator is developed in this work, which can have Good fault tolerance performance, low beginning wind speed, flexible control, etc.

Generally, the power generated from the SRG is AC supply, but when it is connected to the grid system, a constant DC supply is desirable [12]. Therefore, the BR converter is adopted in this study for its small current ripple, constant input current, and enhanced converter reliability with reduced switching losses. Moreover, control techniques are necessary to ensure a stable and regulated voltage for wind energy-based grid applications. Numerous conventional control topologies are utilized for SRG systems. The traditional Proportional plus Integral plus Derivative (PID) and Proportional plus Integral (PI) [13, 14] controllers have essentially been used in a lot of control applications because of their wide stability margin and resilience. However, due to the nonlinearity of dynamic systems and parameter fluctuations, the traditional PI and PID controllers are extremely susceptible [15].

Consequently, in order to attain the intended performance, the appropriate PI parameters are required. Numerous optimization methods have been introduced to tune the PI. In [16], GA, PSO [17], and ABC [18] are the heuristic optimization-based tuning techniques used to raise the effectiveness of the aforementioned controller. When simulating the value of the generations function, GA takes a long time, whereas PSO converges quickly [19]. Compared to PSO, the ABC algorithm provides more precise optimization. Nevertheless, it suffers from inappropriate exploitation while attempting to solve challenging issues [20]. To overcome the above-stated issues, the proposed work implemented a Cat Swarm Optimized PI controller technique, which performs better in settling time with rapid convergence speed than the conventional optimization techniques.

The contributions of the proposed work are illustrated below,

- To reduce greenhouse gas emissions and to operate in an extensive speed range by incorporating SRG in the wind energy system.
- Distribute the DC supply and boost the voltage from the SRG system by implementing a BR converter.
- To stabilize the voltage and to tune the parameter of the PI controller adopting CSO-PI controller.
- To achieve grid synchronization, a PWM generator (Hysteresis controller) is utilized.

2. Proposed Methodology

The cat swarm optimized PI controller is proposed in this work for a wind energy-based switched reluctance generator. As illustrated in Figure 1, the proposed approach seeks to maximize the potential of SRG specially developed for wind energy applications in microgrid networks.

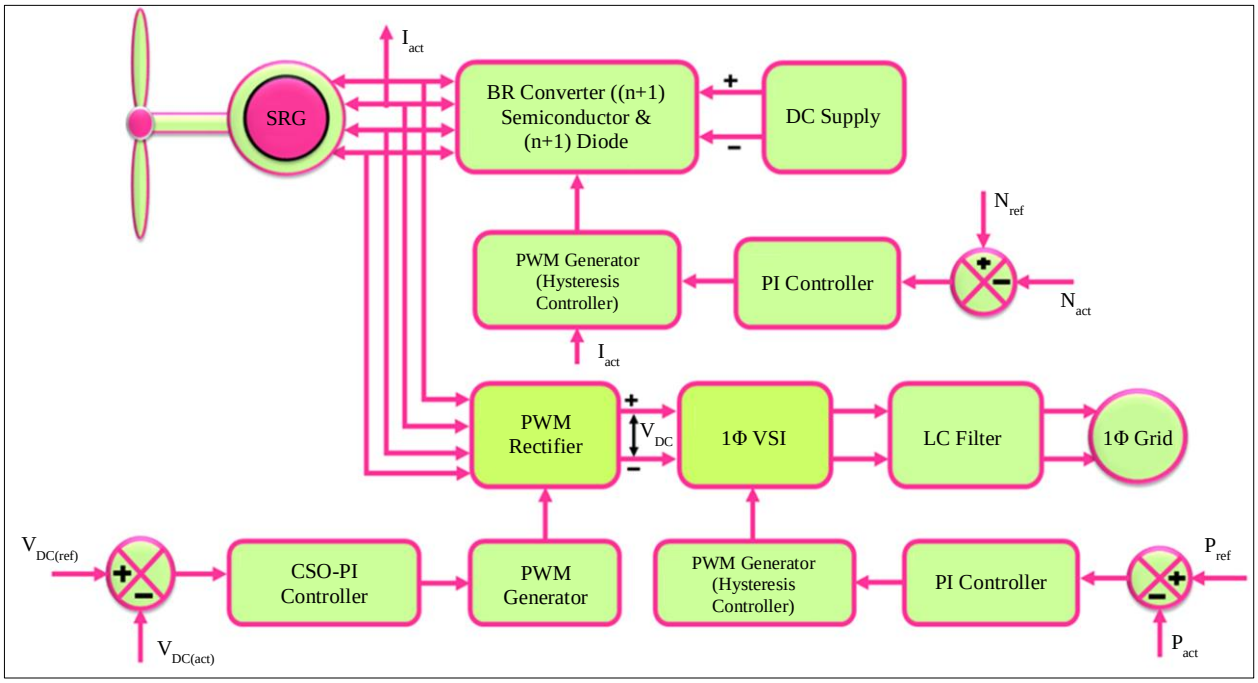

Fig. 1 Block diagram of the proposed method

The wind energy-based SRG system is given as the input source, which generates AC supply, and it is converted into DC by utilizing BR converter $(n+1)$ diode and $(n+1)$ semiconductor topology for the grid applications. The BR converter is regulated by adopting the PI controller, and the controlled output is given to the PWM generator (Hysteresis controller) to generate the necessary pulses for the BR converter to function well. The current from the SRG system is given to the PWM rectifier to convert the AC-DC supply. Moreover, CSO optimized PI controller is used to enhance the parameters of the PI controller, which boosts the performance and efficiency of the controller. The controlled output from the optimized PI controller is delivered to the PWM generator to produce essential pulses for better operation of the rectifier. The reference current is compared with the real current that produced a signal with an error and is served to the PI controller for compensating the error. The constant DC current is given to single-phase VSI to convert DC-AC into the grid system. The PWM generator (Hysteresis controller) controls the VSI and generates the Switching pulses for the VSI. The AC supply is fed to the LC filter, eliminating the harmonics and delivering a single-phase grid system with an uninterruptable and constant power supply.

2.1. Modelling of Wind Turbine-Driven Switched Reluctance Generator

A device that transforms wind energy from kinetic to mechanical form is a wind turbine. The following indicates the mechanical torque, T_m, applied to the wind turbine shaft.

$$T_m = \frac{1}{2}\rho A R \frac{C_P(\lambda)}{\lambda} \quad (1)$$

Where, λ specifies the tip speed ratio, R indicates a turbine blade radius, ρ denotes a density of air, A represents the area swept by the blades, V_w specifies wind speed.

$$\lambda = \frac{R\omega_m}{V_w} \quad (2)$$

The dynamic equation for the generator can be calculated as follows:

$$J\frac{d\omega_m}{dt} = T_m - T_e \quad (3)$$

Where, T_e specifies the total torque generated by the generator phases, J indicates the moment of inertia.

Once the stator of SRG and poles of the rotor are perfectly allied, the phase inductance is at its highest, and the reluctance is lowest. The stator windings' current drops as the rotor pole moves out of alignment, and the inductance approaches its lowest value. The magnetic field in SRG essentially drives the poles towards their minimal reluctance state, which is where torque generation occurs.

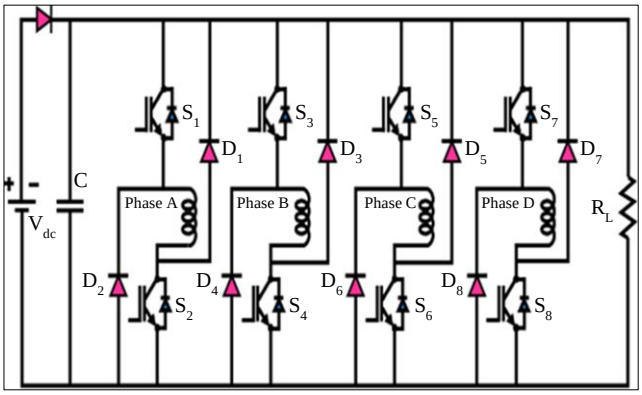

Fig. 2 Circuit diagram of SRG system

Excitation from the SRG is synchronized with the position of the rotor to generate torque. In linear operating circumstances, the torque created by an SRG phase is computed as,

$$T_e = \frac{1}{2} i^2 \frac{dL}{d\theta} \quad (4)$$

Here, i, T_e, θ and L denote the phase current, EM torque, rotor position and phase inductance. The complete torque created by the four-phase generator employed in this investigation is equivalent to the independent addition of the torques formed by each phase.

$$T_e = T_a(\theta, i_a) + T_b(\theta, i_b) + T_c((\theta, i_c)T_d(\theta, i_d) \quad (5)$$

Formula (2) can be utilized to show the total torque. The SRG's torque is negative when the rotor and stator poles are moving apart as a result of the generator's energizing windings. Asymmetric Half Bridge (AHB) converter utilized in this investigation to drive the SRG is depicted in Figure 2. There are two diodes and switches for each phase in this driver circuit.

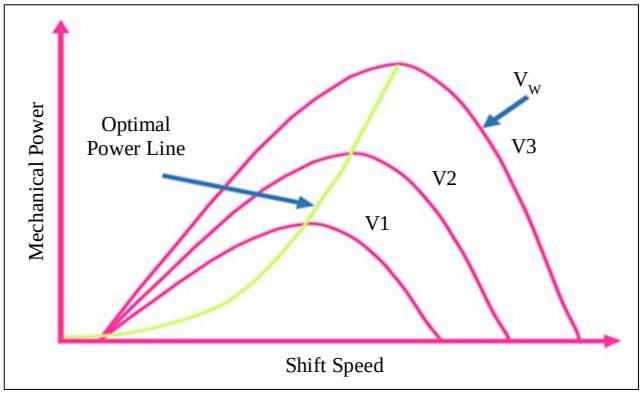

Fig. 3 Wind turbine system's mechanical power curves

The SRG's phase voltage is represented by the equation in,

$$V = R.i + \frac{d\psi}{dt} \quad (6)$$

Here, $R, V, \theta, L \; and \; \psi$ specifies the phase resistance, voltage applied to phase winding, rotor position, phase inductance and magnetic flux.

$$\psi = L(i, \theta).i \quad (7)$$

$$V = R.i + L\frac{di}{dt} + i\frac{d\theta}{dt}\frac{dL}{d\theta} \quad (8)$$

$$\omega = \frac{d\theta}{dt} \quad (9)$$

The voltage equation of the SRG can be rearranged by utilizing the Equations (7), (8), and (9) to provide (10) and (12).

$$V = R.i + L\frac{di}{dt} + i\omega\frac{dL}{d\theta} \quad (10)$$

$$e = \omega.i.\frac{dL}{d\theta} \quad (11)$$

$$V = R.i + L\frac{di}{dt} + e \quad (12)$$

Here, where x is the rotating speed and e is the back electromotive force, as stated in Equation (11).

In the proposed work, the SRG is driven by an external DC source with a BR converter to control and regulate the speed. The following is the modeling of a BR converter with $(n + 1)$ diode and $(n + 1)$ semiconductor topology:

2.2. Modelling of BR Converter

A Bridge Rectifier (BR) converter is utilized to create the converter's output to the Switched Reluctance (SR) motor. One benefit of utilizing this converter is that each phase operates independently, allowing the motor to work on only one phase in the event that the other three phases malfunction. Figure 4 displays the schematic diagram of the BR converter. Each phase of this converter has two diodes and two semiconductor switching components. In this instance, the position of the rotor determines how the windings are powered.

T_1 and T_2 are active when winding A is energized and OFF when the winding is disconnected from the supply. The energy kept in the winding flows over diodes D_1 and D_2 when the device is in the off state, allowing the return current to reach the supply. The subsequent phases likewise follow a similar procedure. It is observed that while using this architecture for high-speed operations, the cached energy needs to be fed into the supply in the allotted amount of time. Typically, the lower leg switches $T2, T4, T6, and \; T8$ are controlled by the chopping frequency signal, while the upper leg switches $T1, T3, T5, and \; T7$ are turned active and OFF based on the location of the rotor. To adjust the angle of conduction θ, appropriate control circuits are employed.

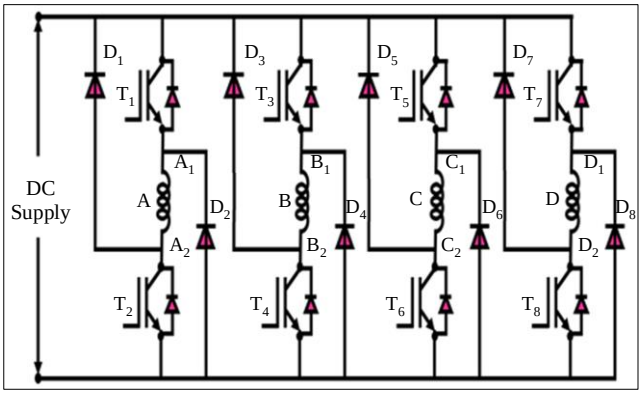

Fig. 4 Circuit diagram of BR converter

2.3. PI Controller

With the derivative control eliminated, the PI controller is a condensed form of the PID controller. P is for proportion, and I stands for integral. Figure 5 displays the structure of the PI controller, and the following equation can be used to characterize the output of a traditional PID controller:

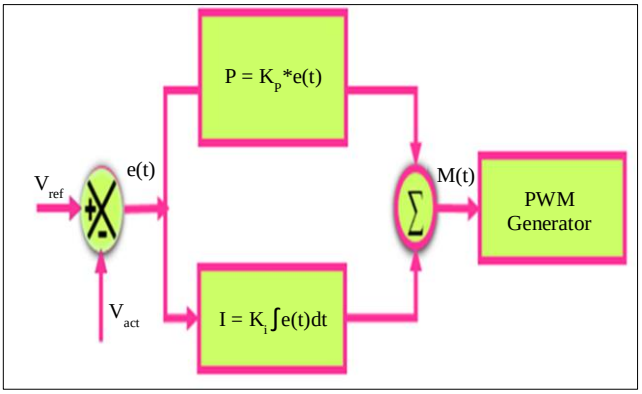

Fig. 5 Schematic diagram for PI controller

$$u(t) = K_P.e(t) + K_i.\int_0^1 e(t)dt, \quad (13)$$

Here, K_P stands for proportional gain, $u(t)$ specifies the output of the PI controller, $e(t)$ denotes speed error and K_i indicates integral gain.

In contemporary control systems, discrete processing is required, and the continuous PI controller should not be used directly for reliability's sake; then the following can be used to express the digital conventional PI controller:

$$u(k) = K_P.e(k) + K_i\sum_{j=0}^{k} e(j) \quad (14)$$

Where, $e(k)$ specifies the error at the time of k. To alter the parameter of this controller, a CSO method is utilized in this proposed work, which is stated below.

2.4. Modelling of Cat Swarm Optimization

The smart algorithm CSO mimics aspects of the behavior of a cat in its natural environment. Both the tracking and seeking modes are distinct behavioral patterns shared by all cats. Searching cats rest for the majority of the day. Like humans, cats are constantly on the lookout and monitoring their environment. When tracking cats locate their prey, they rush swiftly to reach the objective.

Each cat in CSO represents a single solution to the problem that needs to be optimized. Flag, position, and fitness are the three attributes that each cat possesses. The assessment of each cat's positioning is done using fitness. Tracking and seeking behavior patterns of individual cats are distinguished by flags.

In the solution space, the position P_i of the ith cat is defined as a D-dimensional vector. P_i 's jth dimension is denoted byP_{ij}. The velocity (V_{ij}) of $P_{ij}$is unique. According to Equations (15) and (16), the velocity vector (V_i) of the ith cat is then composed of the D-dimensional vector of V_{ij}. D gives dimensions to the solution space.

$$P_i = \{P_{ij}\}, j = 1,2, \dots, D, \quad (15)$$

$$V_i = V_{ij}, j = 1,2, \dots, D. \quad (16)$$

Step 1 : Initialize cat set up cats first. Each cat's position and speed are chosen randomly to create a specific number of cats in D-dimensional solution space.

Step 2 : Set CSO's initial characteristics, including MR SRD, as well as the velocity's inertia value (ω).

Step 3 : Determine the cats' level of fitness. Every cat's fitness is computed, and the best fitness is noted in pbest.

Step 4 : Cats should be divided. Cats are arbitrarily assigned to tracking or seeking modes based on the mixture rate. The tracking and seeking procedures are carried out based on the cat's flag.

Step 5 : Update the cats' level of fitness. Each cat's fitness value is recalculated after the tracking and seeking processes are finished. The value of optimal fitness is documented in pl.

Step 6 : Pbest is updated. Contrast PL with pbest. Update pbest with the superior option.

Step 7 : The algorithm ends if the end condition is satisfied; if not, repeat steps 4 through 7 again

2.4.1. Seeking mode

Cats spend most of their time sleeping when in the searching phase. But cats are always aware of their surroundings and also keep an eye on things. The cat always cautiously and slowly shifts to a new position after surveying its surroundings if it wants to change positions.

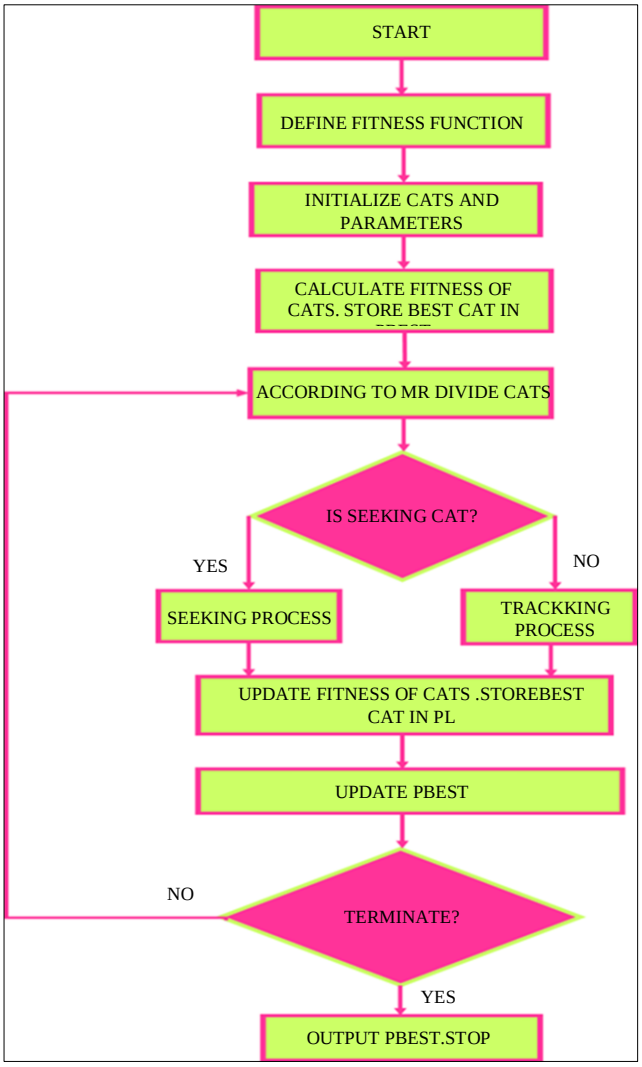

Fig. 6 Flowchart of CSO

The CSO's seeking mechanism mimics a cat's natural tendency to find its next location. In the searching mode, there are 3 important parameters. The term "Seeking Memory Pool" (SMP) refers to the extent of each cat's seeking memory, which is utilized to store every location a cat is capable of remembering.

SRD: It specifies the range of values that can be altered for every cat position dimension.

Dimensions to change (CDC): This indicates how many dimensions of a cat's position are subject to mutation. The solution space dimension (D) cannot be exceeded by the number.

The procedure for seeking is as follows.

Step 1 : Transfer K replicas of the ith cat to the SMP in searching mode (K = SMP).

Step 2 : Maintain one copy of each of the K copies. Additionally, K − 1 copies experience mutation. Based on CDC (Equation (15), each cat in K − 1 replicas randomly adds or subtracts SRD percent's of the current position value.

$$P_{ij} = (1 \pm SRD)\circledR P_{ij}, P_{ij} \in P_i \quad (17)$$

Step 3 : In SMP, determine each copy's fitness by updating it.

Step 4 : Select the K copies with the highest fitness, then use that copy to replace the cat in that location.

2.4.2. Mode of Seeking

When a cat detects prey, it will seek the target swiftly while in tracking mode. To maintain their progress towards the target, each cat will modify their position by adjusting their movement speed.

The procedure for tracking is as follows:

First, update the ith cat's speed in tracking mode using Equation (16). In complete cats, pbest j denotes the j^{th} dimension of the best cat. ω specifies the value of inertia. c indicates a preset constant between 0 and 2, and rand is a random number with uniform distribution [0, 1].

$$V_{ij} = \omega \times V_{ij} + rand \times c \times (pbest_j - P_{ij}), j = 1,2, \dots, D \quad (18)$$

Ensure the updated cat speed stays within the permitted speed range in step two.

Step 1 : Using Equation (17), update the with cat's position in the tracking mode.

$$P_{ij} = P_{ij} + V_{ij}, j = 1,2, \dots D. \quad (19)$$

With the implementation of the cat swarm optimization algorithm, the parameter of PI (K_p, K_i) controller tuned efficiently. The performance of the PWM generator was further enhanced using the hysteresis current controller, which is explained in the section below.

2.5. Modelling of Hysteresis Controller

Hysteresis Current Controller (HCC) is schematically represented in Figure 7 and receives the reference current that is thus acquired from the PI controller. This control is used because current chopping regulates the current flowing through the stator winding while the motor operates at a low speed when the back-emf is low. The PI controller analogizes the actual and reference speeds and feeds the resulting reference signal to the HCC. The commutation controller determines the phase to be switched ON by taking the position from the position sensor. Thus, $\theta_{ON}, \theta_{OFF}$ the HCC receives the actual current and the reference signal from the PI.

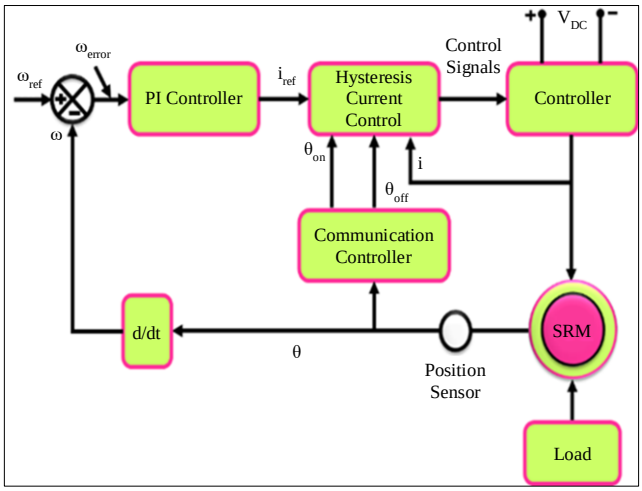

Fig. 7 Schematic diagram of HCC controller

The major goal of using a HCC is to keep the current inside the hysteresis band (Δi) during the conduction phase. When the two currents are compared, the pure form of the current is removed, resulting in ripples that are supplied into the BR converter, where they are transformed into pulses.

3. Results and Discussion

This work proposes a wind energy-based switched reluctance generator with a cat swarm optimized PI controller for a grid distributing system. By using the BR converter, the output voltage from the SRG is competently enhanced, and the efficiency of the PI controller is superior in performance by assisting the cat swarm optimization technique. Furthermore, the total proposed work is executed in MATLAB, and a comparison is made with the existing technique to demonstrate the ability of the proposed work. Table 1 represents the parameter ratings, which are shown below.

Table 1. Parameter specification

Parameters	Specifications
SRG	
Rated Power	10KW
Number of Stato / Rotor Poles	8/6
Rated Voltage	310V
Speed	6000rpm
Rated Power	10KW
Saturated Aligned Inductance	$0.15e^{-3}$H
Aligned Inductance	$23.6e^{-3}$H
Unaligned Inductance	$0.67e^{-3}$H
Switch	IGBT
Driver Circuit	TL250

3.1. Case 1

The PWM rectifier's waveform utilizing PI and CSO-PI controller is represented in Figure 8, which is observed that initially, the voltage is peakly raised and becomes constant at 300V after 0.5s by using the PI controller as specified in Figure 8(a). Similarly, the voltage is raised suddenly and maintained constant at 300V after 0.3s using the CSO-PI controller, as represented in Figure 8(b).

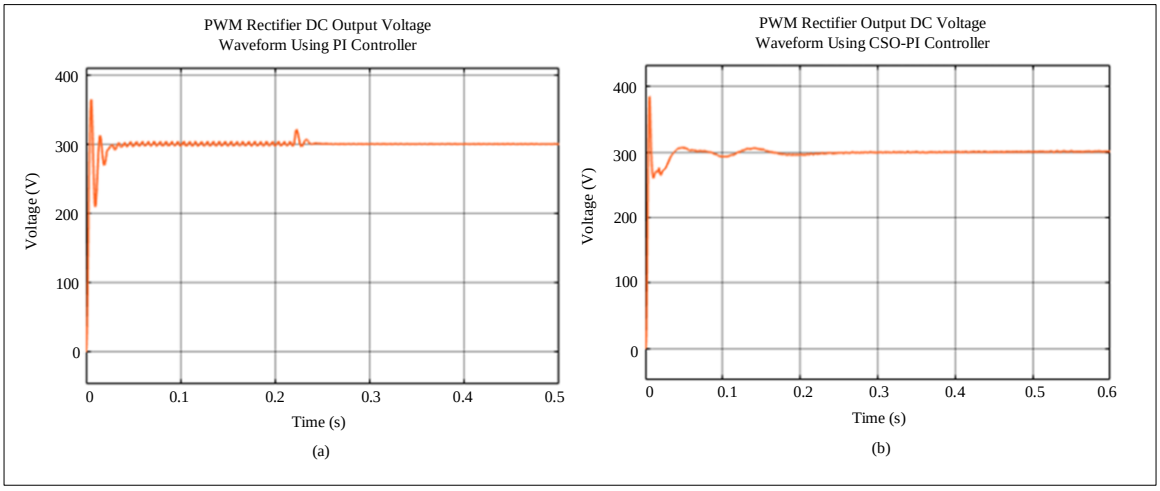

Fig. 8 Output voltage waveform for PWM rectifier utilizing (case 1) (a) PI, and (b) CSO-PI controller.

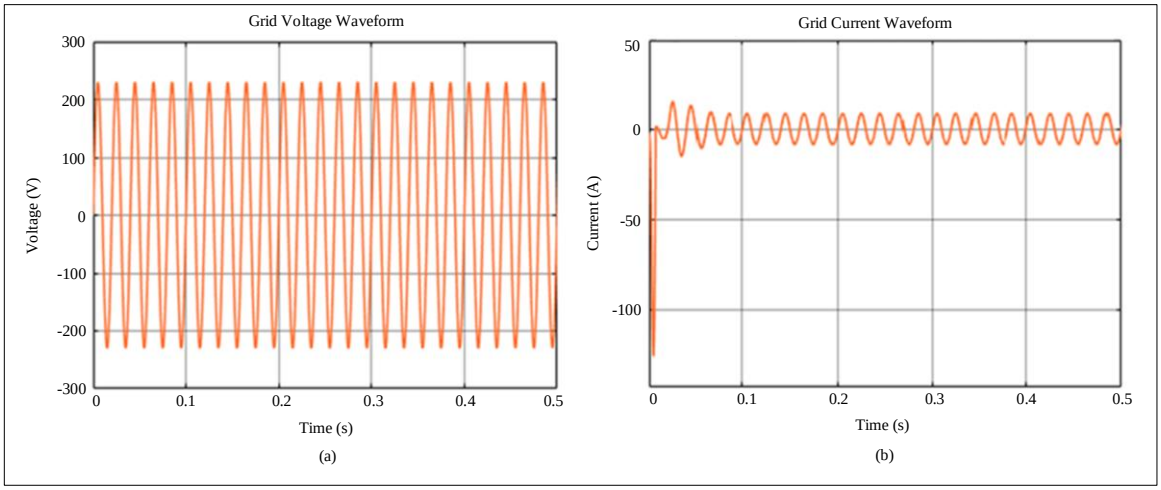

Fig. 9 Waveform for grid (case 1) (a) Voltage, and (b) Current.

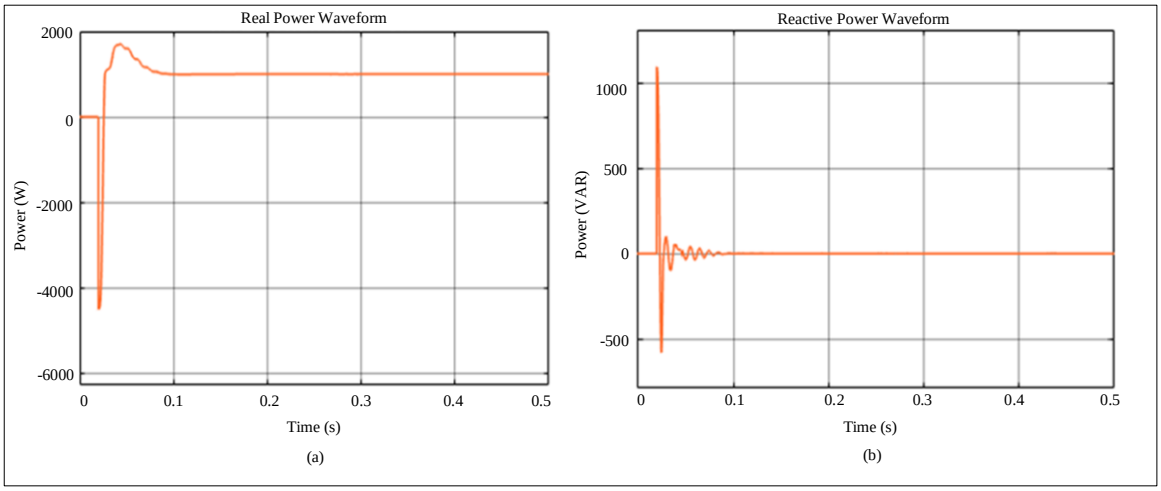

Fig. 10 Waveform for (case 1) (a) Real, and (b) Reactive power.

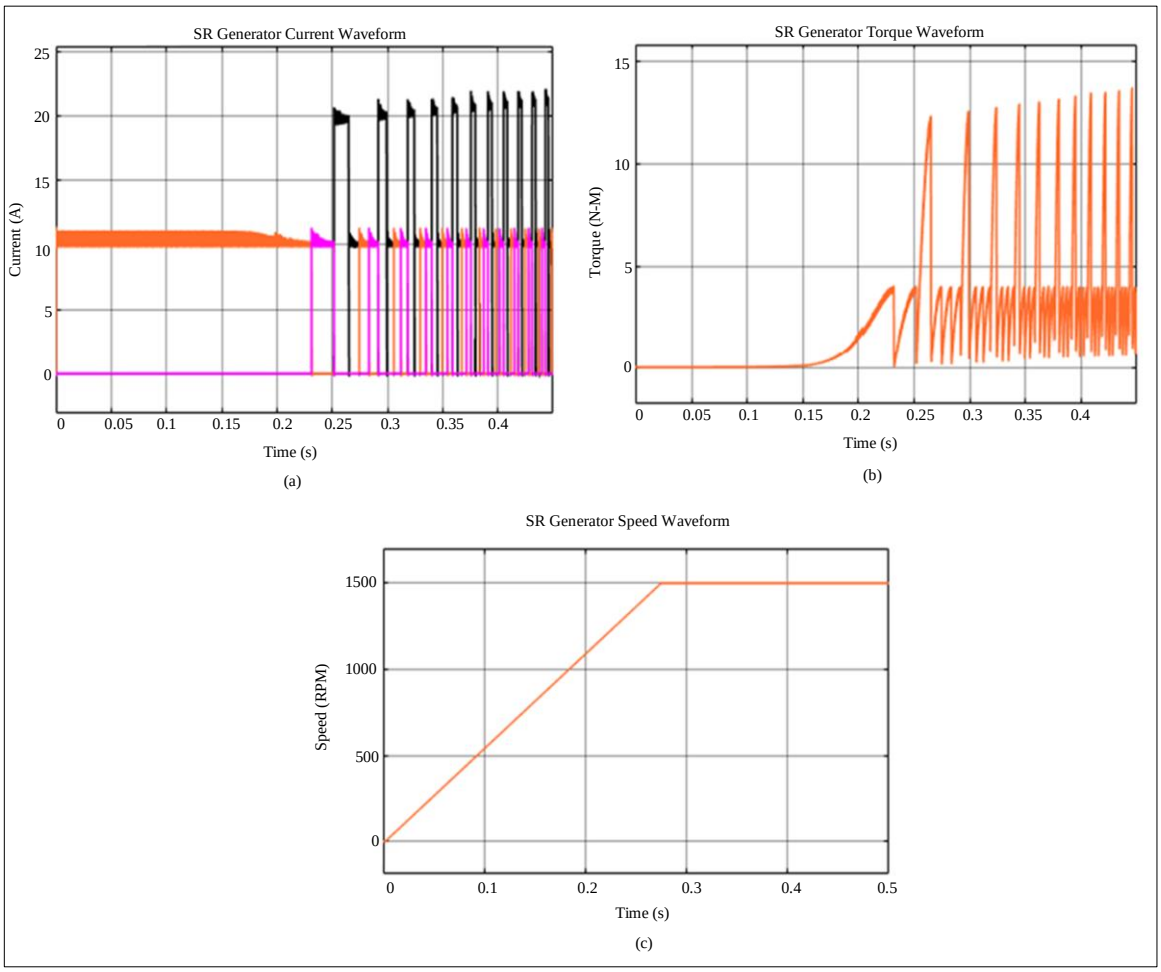

Fig. 11 Waveform for SR generator (case 1) (a) Current, (b) Torque, and (c) Speed.

Figure 9 represents the waveform for grid voltage and current; from the results, it is analyzed that the voltage is continuously sustained at 220 to -220, and the current is peakly raised and 0A with distortion as specified in Figure 9 (b). The waveform for real and reactive power is illustrated in Figure 10, which noted that the real power is peakly raised and becomes constant at 3000W, as represented in Figures 10(a) and 10(b), which illustrates the reactive power is suddenly raised at 0VAR respectively.

The waveform for the SR generator with current, torque and speed is represented in Figure 11. Initial stabilization of the current is observed after 0.2s with minor distortions, as represented in Figure 11(a). Similarly, in Figure 11(b), oscillation arises at the initial stage, followed by a rise and fall in torque level after 0.25s. From the graph, it is clear that the speed of the SR generator was raised to a peak level and maintained constantly at 1500RPM after 0.3s.

3.2. Case 2

Figure 12 illustrates the PWM rectifier's waveform utilizing PI and CSO-PI controller; from the result, it is observed that initially, the voltage is peakly raised and becomes constant at 300V after 0.3s by the use of PI controller as specified in Figure 12(a). Similarly, the voltage is raised suddenly and maintained constant at 300V after 0.25s using the proposed CSO-PI controller, as represented in Figure 12(b).

The waveform for grid current and voltage is represented in Figure 13; from the results, it is evaluated that the voltage is continuously sustained at +220 to -220, and the current is peakly raised and sustained at 0A with distortion as specified in Figure 13(b).

Figure 14 specifies the waveform for real and reactive power, which is observed that the real power is peakly high and becomes constant at 3000W as represented in Figures 14(a), and 14(b) represents the reactive power waveform, which is suddenly raised and maintained constant at 0VAR respectively.

Figure 15 shows the SR generator's waveform with current, Flux, torque, and speed. After 0.2 seconds, the current

begins to stabilize initially with just slight distortions, as specified in Figure 15(a). In a similar manner, oscillation appears at the beginning of Figure 15(c) and ends with a rise and decrease in torque level after 0.25 seconds. It is evident from the graph that the SR generator's speed increased to a maximum and remained there for 0.2 seconds at 1000 RP.

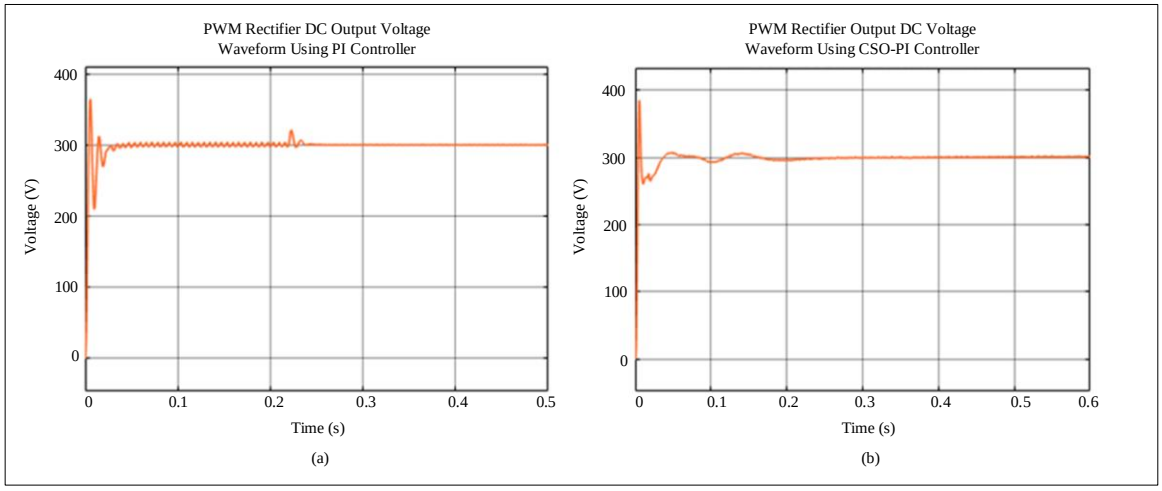

Fig. 12 Output voltage waveform for PWM rectifier using (case 2) (a) PI, and (b) CSO-PI controller.

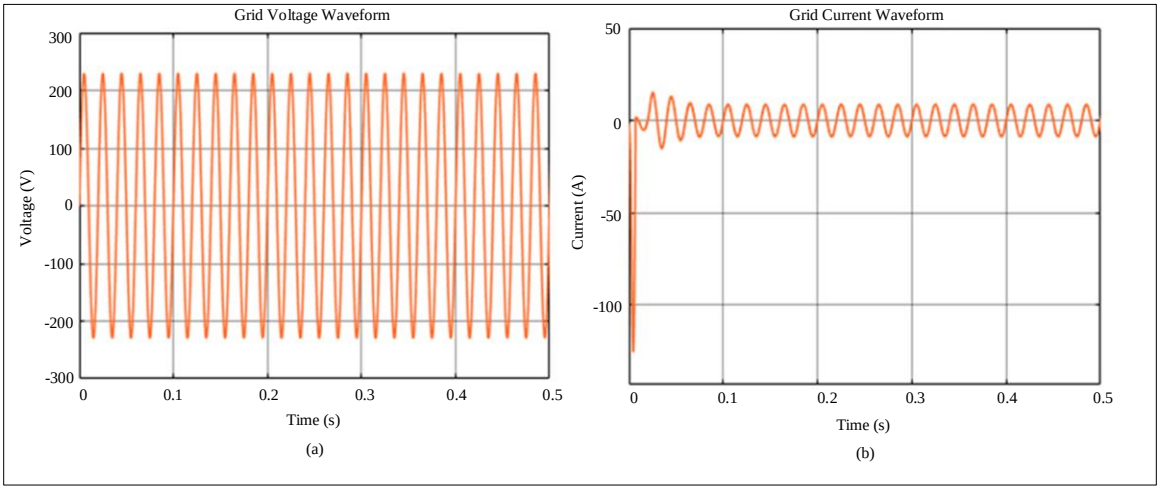

Fig. 13 Waveform for the grid (case 2) (a) Voltage, and (b) Current.

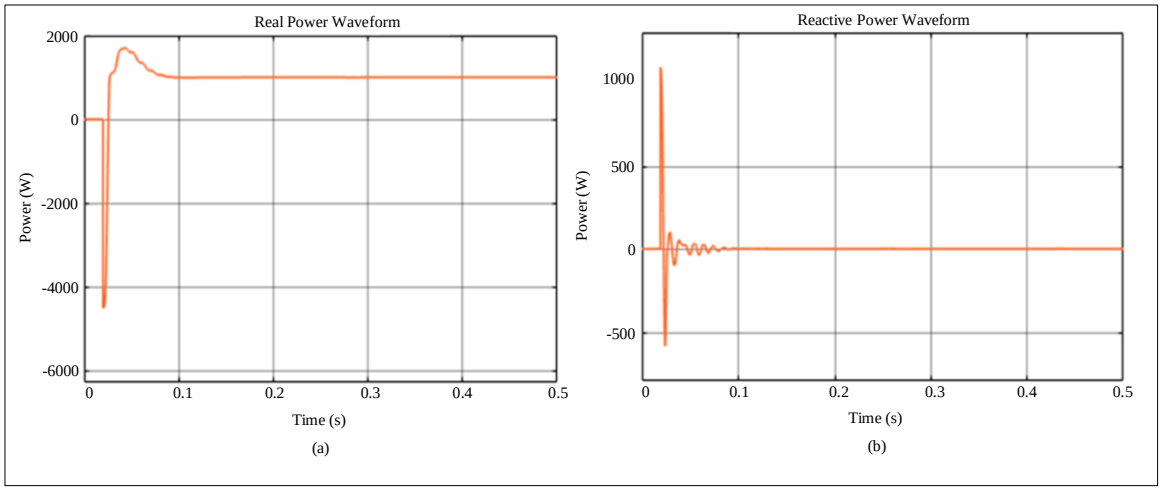

Fig. 14 Waveform for (case 2) (a) Real, and (b) Reactive power.

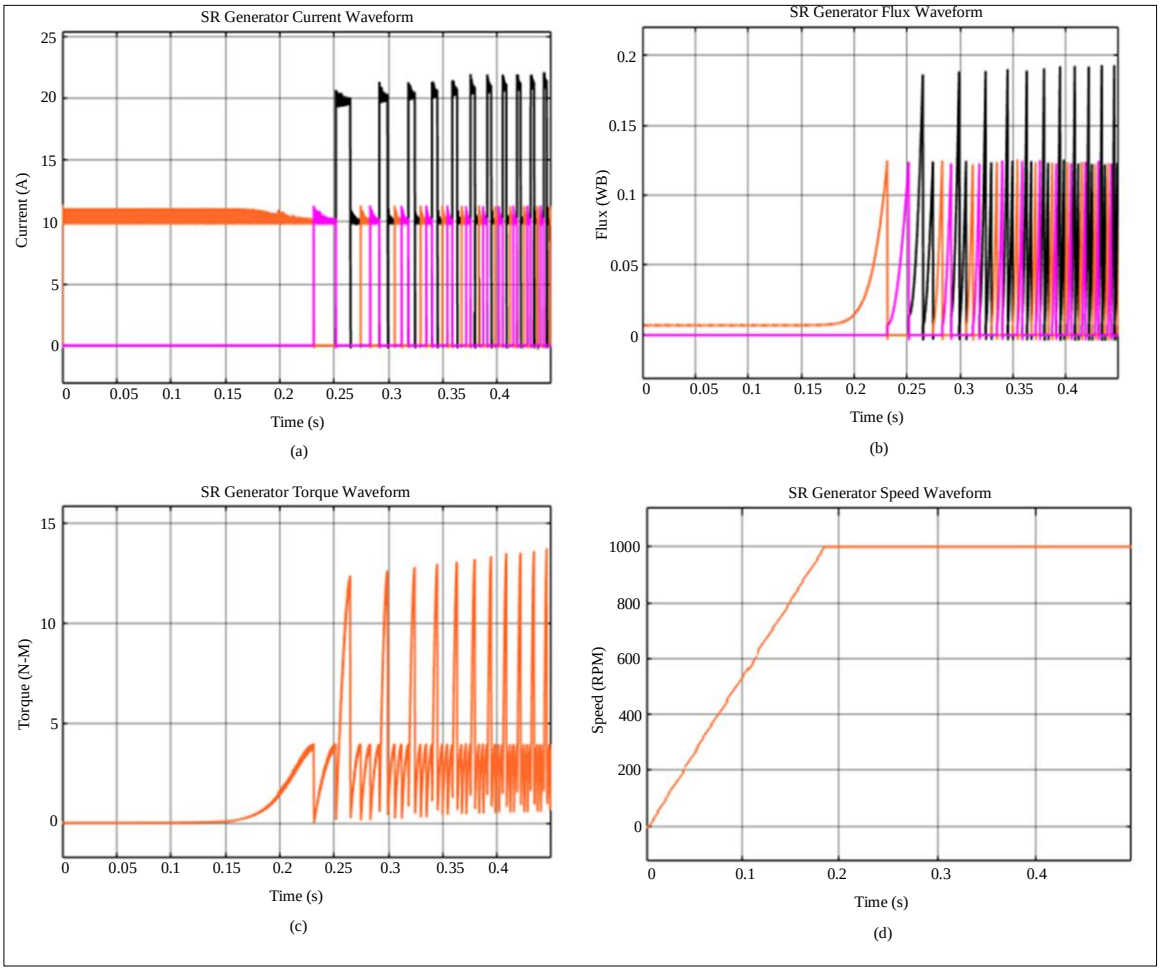

Fig. 15 Waveform for SR generator (case 2) (a) Current, (b) Flux, (c) Torque and (d) Speed.

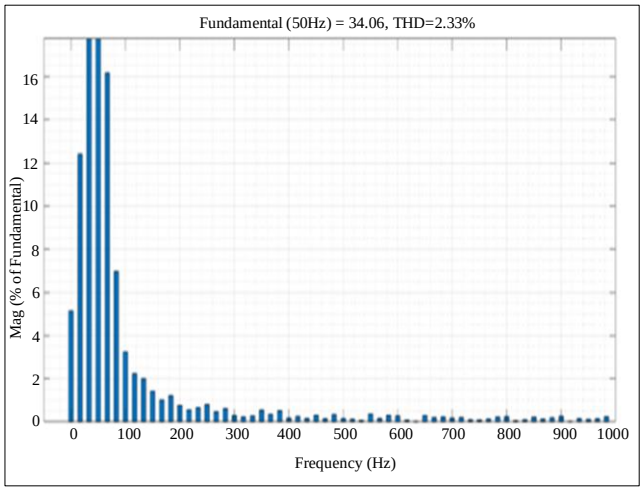

Fig. 16 THD waveform

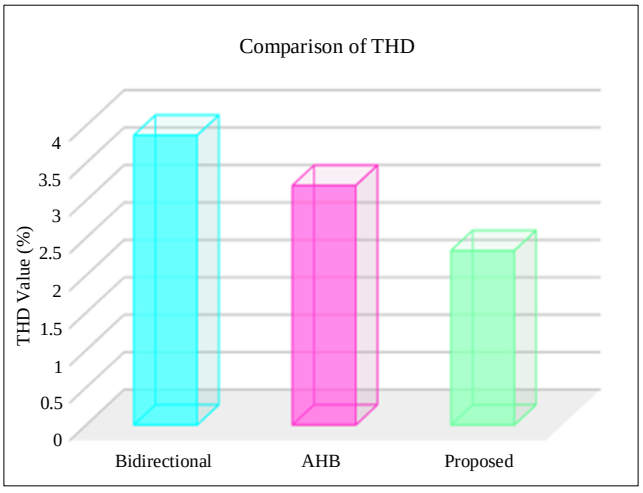

Fig. 17 THD value comparison

The waveform of THD for the proposed approach is displayed in Figure 16, from which it is analyzed that the developed work attains a 2.33% THD value.

A comparison of THD value is signified in Figure 17; from the graph, it is examined that the proposed converter is compared with the traditional AHB converter. The proposed

BR converter achieves a low THD value of 2.33% compared to the other existing converters.

Table 2. Comparison of dynamic performance

Optimized PI Controller	Settling Time (s)	Rise Time (s)
PI	0.3	0.01
PSO-PI [21]	0.35	0.15
ASO-PI [22]	0.26	0.08
CSO- PI	0.25	0.01

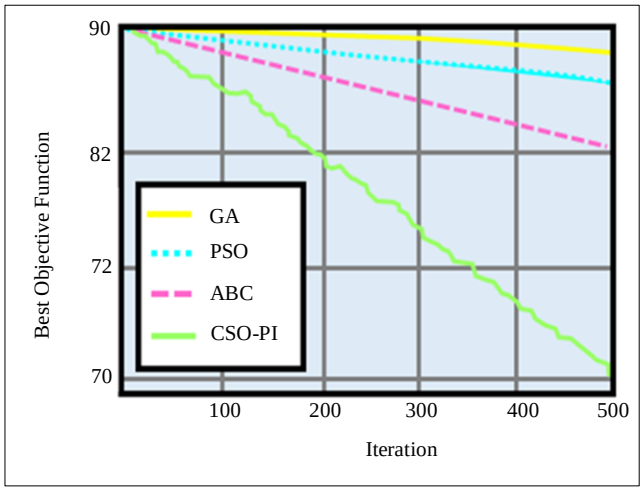

Fig. 18 Comparison of convergence speed

The Proposed CSO optimized PI controller is compared with the conventional techniques, as demonstrated in Table 2. From the table, it is analyzed that the proposed optimized controller attains a tremendous rise time and settling time compared to the existing techniques. Figure 18 represents the convergence speed of the algorithms with the maximum iteration number. The efficiency of the developed system is systematically enriched by the CSO-PI approach in addition to GA, PSO and ABC. Moreover, the proposed has a fast convergence rate with a small iteration number.

4. Conclusion

The wind energy-based switched reluctance generator with cat swarm optimized PI controller is proposed for the grid distributing system. The SRG system makes sense due to its resilience, wide speed range, ease of maintenance and ability to function in challenging conditions. By integrating the PI controller, the speed of SRG is effectually controlled, which adjusts the output current of the BR converter ($n+1$ diode and $n+1$ semiconductor system.

The PWM generators (Hysteresis controllers) are used to manage VSIs by generating switching pulses for the device based on an instantaneous comparison between the grid current and the reference current. Moreover, the Cat Swarm Optimization technique is competently tuned to the PI controller, improving the developed controller's performance and efficiency.

Finally, the overall implemented technique is executed in MATLAB, and a comparison is made between the traditional methods to foresee the significance of the proposed work. From the comparison graph, it is analyzed that the implemented optimized controller attains a low THD of 2.33%, a rapid Settling time of 0.25s, and a convergence speed with effective grid synchronization.

Reference

[1] K.S. Kavin, and P. Subha Karuvelam, "PV-Based Grid Interactive PMBLDC Electric Vehicle with High Gain Interleaved DC-DC SEPIC Converter," *IETE Journal of Research*, vol. 69, no. 7, pp. 4791-4805, 2021. [CrossRef] [Google Scholar] [Publisher Link]

[2] Kaniz Farhana et al., "Energy Consumption, Environmental Impact, and Implementation of Renewable Energy Resources in Global Textile Industries: An Overview towards Circularity and Sustainability," *Materials Circular Economy*, vol. 4, no. 1, 2022. [CrossRef] [Google Scholar] [Publisher Link]

[3] Sebastian Rivera et al., "Bipolar DC Power Conversion: State-of-the-Art and Emerging Technologies," *IEEE Journal of Emerging and Selected Topics in Power Electronics*, vol. 9, no. 2, pp. 1192-1204, 2021. [CrossRef] [Google Scholar] [Publisher Link]

[4] Nima Rezaei et al., "A Novel Hybrid Machine Learning Classifier-Based Digital Differential Protection Scheme for Intertie Zone of Large-Scale Centralized DFIG-Based Wind Farms," *IEEE Transactions on Industry Applications*, vol. 56, no. 4, pp. 3453-3465, 2020. [CrossRef] [Google Scholar] [Publisher Link]

[5] Hao Chen, Deguang Xu, and Xin Deng, "Control for Power Converter of Small-Scale Switched Reluctance Wind Power Generator," *IEEE Transactions on Industrial Electronics*, vol. 68, no. 4, pp. 3148-3158, 2021. [CrossRef] [Google Scholar] [Publisher Link]

[6] Qin Jiang et al., "Time-Sharing Frequency Coordinated Control Strategy for PMSG-Based Wind Turbine," *IEEE Journal on Emerging and Selected Topics in Circuits and Systems*, vol. 12, no. 1, pp. 268-278, 2022. [CrossRef] [Google Scholar] [Publisher Link]

[7] José Luis Torres-Madroñero et al., "Technological and Operational Aspects that Limit Small Wind Turbines Performance," *Energies*, vol. 13, no. 22, 2020. [CrossRef] [Google Scholar] [Publisher Link]

[8] V.B Murali Krishna et al., "Experimental Investigation on Performance Comparison of Self-Excited Induction Generator and Permanent Magnet Synchronous Generator for Small Scale Renewable Energy Applications," *Renewable Energy*, vol. 195, pp. 431-441, 2022. [CrossRef] [Google Scholar] [Publisher Link]

[9] Xianxian Zhao, Ying Xue, and Xiao-Ping Zhang, "Fast Frequency Support from Wind Turbine Systems by Arresting Frequency Nadir Close to Settling Frequency," *IEEE Open Access Journal of Power and Energy*, vol. 7, pp. 191-202, 2020. [CrossRef] [Google Scholar] [Publisher Link]

[10] Ali Dali et al., "A New Robust Control Scheme: Application for MPP Tracking of a PMSG-Based Variable-Speed Wind Turbine," *Renewable Energy*, vol. 172, pp. 1021-1034, 2021. [CrossRef] [Google Scholar] [Publisher Link]

[11] Hossein Ehya, and Jawad Faiz, *Electromagnetic Analysis and Condition Monitoring of Synchronous Generators*, Wiley-IEEE Press, 2022. [Google Scholar] [Publisher Link]

[12] Pedro José dos Santos Neto et al., "Grid-Connected SRG Interfaced with Bidirectional DC-DC Converter in WECS," *IEEE Transactions on Energy Conversion*, vol. 36, no. 4, pp. 3261-3270, 2021. [CrossRef] [Google Scholar] [Publisher Link]

[13] Zeineb Touati et al., "Improvement of Steady State Performance of Voltage Control in Switched Reluctance Generator: Experimental Validation," *Machines*, vol. 10, no. 2, 2022. [CrossRef] [Google Scholar] [Publisher Link]

[14] Padmashree V. Kulkarni, H.V. Govindaraju, and S. Babitha, "Comparative Analysis of Different Controllers for Adjustable Speed Switched Reluctance Motor Using Closed Loop Operation," *International Journal of Intelligent Systems and Applications in Engineering*, vol. 11, no. 4, pp. 132-140, 2023. [Publisher Link]

[15] T. Dharma Raj et al., "Load Frequency Control in Two-Area Multi-Source Power System Using Bald Eagle-Sparrow Search Optimization Tuned PID Controller," *Energies*, vol. 16, no. 4, 2023. [CrossRef] [Google Scholar] [Publisher Link]

[16] Kaikai Diao et al., "Multimode Optimization of Switched Reluctance Machines in Hybrid Electric Vehicles," *IEEE Transactions on Energy Conversion*, vol. 36, no. 3, pp. 2217-2226, 2021. [CrossRef] [Google Scholar] [Publisher Link]

[17] Mohamed M. Sedky et al., "Integrated Switched Reluctance Starter/Generator for Aerospace Applications: Particle Swarm Optimization for Constant Current and Constant Voltage Control Designs," *Applied Sciences*, vol. 12, no. 15, 2022. [CrossRef] [Google Scholar] [Publisher Link]

[18] Khaoula Belhaj Soulami et al., "An Evaluation and Ranking of Evolutionary Algorithms in Segmenting Abnormal Masses in Digital Mammograms," *Multimedia Tools and Applications*, vol. 79, pp. 18941-18979, 2020.

[19] E. Mirsadeghi, and S. Khodayifar, "Hybridizing Particle Swarm Optimization with Simulated Annealing and Differential Evolution," *Cluster Computing*, vol. 24, pp. 1135–1163, 2021. [CrossRef] [Google Scholar] [Publisher Link]

[20] Mina Javanmard Goldanloo, and Farhad Soleimanian Gharehchopogh, "A Hybrid OBL-Based Firefly Algorithm with Symbiotic Organisms Search Algorithm for Solving Continuous Optimization Problems," *The Journal of Supercomputing*, vol. 78, no. 3, pp. 3998-4031, 2022. [CrossRef] [Google Scholar] [Publisher Link]

[21] Mahidur R. Sarker et al., "dSPACE Controller-Based Enhanced Piezoelectric Energy Harvesting System Using PI-Lightning Search Algorithm," *IEEE Access*, vol. 7, pp. 3610-3626, 2018. [CrossRef] [Google Scholar] [Publisher Link]

[22] Veeramani Bagyaveereswaran, and Pachiyappan Arulmozhivarman, "Gain Scheduling of a Robust Setpoint Tracking Disturbance Rejection and Aggressiveness Controller for a Nonlinear Process," *Processes*, vol. 7, no. 7, 2019. [CrossRef] [Google Scholar] [Publisher Link]